processes

MDPI

Article

Evaluation of Sapucaia (*Lecythis pisonis* Cambess) Shell as a Natural Biosorbent for Chloroquine Removal in Sustainable Water Treatment

Mariana Fernandes Rocha [1], Grace Anne Vieira Magalhães-Ghiotto [1], Anna Carla Ribeiro [1], Felipe Burali Bergamasco [2], Letícia Nishi [2], João Victor Baddini [2], Rosângela Bergamasco [2,*] and Raquel Guttierres Gomes [3]

[1] Department of Biotechnology, Genetics and Cell Biology, Center of Biological Sciences, State University of Maringa, Maringa 87020-900, Parana, Brazil; gvieiramagalhaes@gmail.com (G.A.V.M.-G.)
[2] Department of Chemical Engineering, Technology Center, State University of Maringa, Maringa 87020-900, Parana, Brazil; joaobaddini11@gmail.com (J.V.B.)
[3] Department of Food Engineering, Technology Center, State University of Maringa, Maringa 87020-900, Parana, Brazil
* Correspondence: rbergamasco@uem.br

Abstract

Chloroquine (CQN) is a persistent emerging contaminant whose environmental footprint expanded significantly following its large-scale and off-label use during the SARS-CoV-2 pandemic. Conventional water treatment systems do not effectively remove CQN, and its accumulation in aquatic environments poses risks to ecological balance and public health. This study reports, for the first time, the use of Sapucaia (*Lecythis pisonis* Cambess) shell powder (SPC), an underexplored agro-industrial residue native to the Amazon region and Atlantic Forest, as a biosorbent for CQN removal from aqueous solutions. Physicochemical characterisation revealed a predominantly amorphous material with a strongly negative surface and abundant carboxylic, phenolic, and hydroxyl groups, providing favourable sites for interactions with CQN. Adsorption kinetics were best described by the pseudo-second-order model (R^2 = 0.966), while the Weber–Morris model indicated a three-stage mass-transfer process. Isotherm analysis showed comparable fits for the Langmuir and Freundlich models, with a maximum experimental adsorption capacity of 97.26 mg g^{-1} and a Langmuir-fitted q_{max} of 293.69 mg g^{-1}, both at 298 K. Post-adsorption zeta potential measurements showed a marked neutralisation of the surface charge, supporting the contribution of electrostatic attraction to CQN uptake. After four adsorption–desorption cycles at 26.05 mg L^{-1} using water as the sole desorbent, SPC retained approximately 65% of its initial adsorption capacity, although lower retention was observed at higher adsorbate loadings. Overall, these findings highlight SPC as a low-cost and environmentally friendly biosorbent with promising potential for sustainable water treatment.

Keywords: lignocellulosic biosorbent; agro-industrial residue; pharmaceutical contaminants; adsorption isotherms; wastewater treatment

Check for updates

Academic Editor: Wen-Tien Tsai

Received: 12 August 2026
Revised: 12 September 2026
Accepted: 18 September 2026
Published: 23 September 2026

Copyright: © 2026 by the authors. Licensee MDPI, Basel, Switzerland. This article is an open access article distributed under the terms and conditions of the Creative Commons Attribution (CC BY) license.

1. Introduction

The global proliferation of pharmaceutical contaminants in aquatic environments has become one of the most pressing challenges in environmental management and water treatment science [1,2]. Among these emerging pollutants, chloroquine (CQN), an antimalarial

and immunomodulatory agent with a long history of clinical use [3,4], gained renewed relevance during the SARS-CoV-2 pandemic, as it was widely administered in both developed and developing countries as a candidate treatment [5–8]. Although the World Health Organization subsequently concluded that CQN is ineffective against SARS-CoV-2 and significant adverse effects, including carcinogenic and teratogenic potential, have been documented [9–11], consumption of CQN in Brazil increased by approximately 126% in 2020, generating a corresponding surge in the discharge of pharmaceutical residues into the environment [12–14].

Most pharmaceuticals, such as chloroquine, are not fully metabolised by the human body and are excreted in faeces and urine either in their active form or as metabolites [2,15]. It is estimated that over 20% of the pollutant load discharged to water bodies and wastewater streams results from the discharge of pharmaceuticals and dyes into aquatic systems [16,17]. During the pandemic, large quantities of drug residues generated from pharmaceutical plants, hospitals and households were therefore released into the aquatic environment, where they have been detected at concentrations in the ng L^{-1} range or above [18,19].

As CQN resists conventional water treatment methods, its accumulation in aquatic environments risks accelerating the proliferation of chloroquine-resistant *Plasmodium* strains, with direct consequences for ecological balance and human health [20,21]. The persistence of CQN in water matrices constitutes a long-term environmental hazard that demands effective remediation strategies.

Among the available water remediation technologies, adsorption stands out as a feasible method owing to its efficiency, simplicity, versatility, low cost and sustainability [1,22]. Carbon-based materials [23,24], inorganic materials [25,26] and organic polymers [27–30] are among the materials that have been used for the adsorptive removal of CQN. Among these, the use of agro-industrial residues as adsorbents is an attractive alternative, as it transforms waste into functional materials and combines sustainability with economic accessibility [31]. In this context, biosorbents derived from nutshells, which are rich in cellulose, hemicellulose, lignin, and tannins, have demonstrated competitive adsorption performance for a range of emerging contaminants [32,33].

Lecythis pisonis Cambess (Lecythidaceae), commonly known as Sapucaia, is a tree species native to the Amazon region and Atlantic Forest of Brazil, which also occurs in Colombia, Venezuela, and the Guianas, and whose shell may serve as an alternative biosorbent. Sapucaia nuts are nutritionally similar to Brazil nuts (*Bertholletia excelsa*) and have a chemical composition that varies with the cultivation site, harvesting, and production conditions [34]. In addition, the species is of economic and ecological importance, since it is often used to shade cocoa plantations in Brazilian agroforestry systems. The nutshell, characterised by a hard, dark outer layer, is generated in large quantities as a processing by-product and is routinely discarded without valorisation [34].

While prior research on *Lecythis pisonis* has focused predominantly on the anatomical, morphological, and physiological properties of the plant [33,35–38] and only limited investigations have examined its applications in traditional medicine and food science [38], no study has yet investigated the adsorptive potential of Sapucaia shell for water treatment or pollutant removal purposes. The chemical profile of the *Lecythis pisonis* shell corresponds closely to the surface chemistry that governs effective pharmaceutical adsorption in related nutshell biosorbents [33]. Moreover, the abundance and low cost of this residue in Brazilian agroforestry systems make it a particularly attractive candidate for resource-efficient water treatment applications.

This study therefore evaluates, for the first time, the performance of Sapucaia shell powder (SPC) as a biosorbent for chloroquine removal from synthetic aqueous solutions, through comprehensive physicochemical characterisation and batch adsorption experiments investigating the influence of adsorbent dosage, pH, contact time, temperature, and ionic strength, as well as an assessment of reusability under environmentally compatible regeneration conditions.

2. Materials and Methods

2.1. Materials

Deionised water, HCl (Nuclear), NaOH (Dinâmica, ≥98.0%), and NaCl (Anidrol, ≥99.0%).

2.1.1. Adsorbate

For the adsorption experiments, the pharmaceutical compound chloroquine phosphate (compounding pharmacy, Maringa, PR, Brazil, purity ≥ 98.5%) was dissolved in deionised water and its initial and final concentrations were determined using a UV–Vis spectrophotometer (DR 6000, Hach, Loveland, CO, USA) at a wavelength of 343 nm. The physicochemical properties of chloroquine are summarised in Figure 1. In aqueous solution, chloroquine phosphate dissociates into protonated chloroquine and phosphate counterions. Since chloroquine has a pK_a of 10.32, the cationic form predominates over the pH range investigated [24].

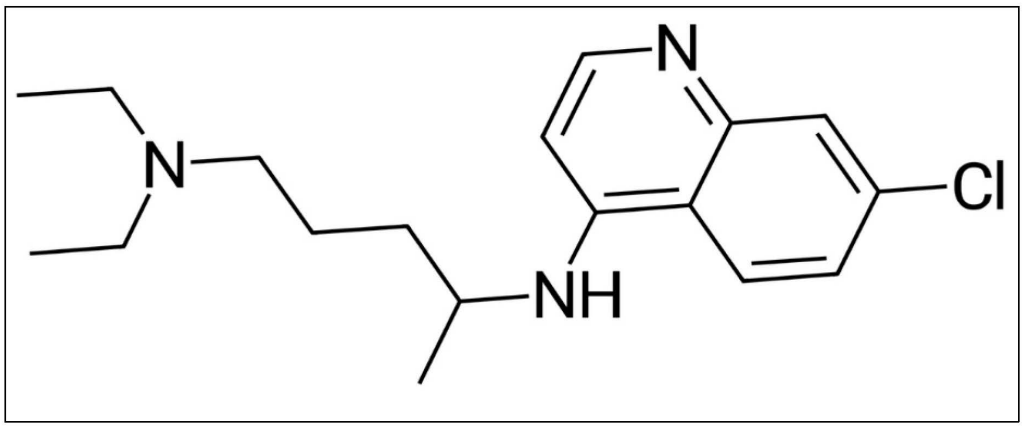


Figure 1. Chemical structure of chloroquine ($C_{18}H_{26}ClN_3$; molecular weight 319.87 g mol^{-1}; pK_a 10.32).

2.1.2. Adsorbent Preparation

Sapucaia (*Lecythis pisonis* Cambess) nutshell samples used in the experiments were collected from a smallholding in Vitória, ES, Brazil. The shells were removed manually using a stainless-steel nutcracker and washed repeatedly with deionised water at approximately 333 K to remove adhering dirt. The material was then dried in an oven (Digital Time, Sterilifer, Sao Caetano do Sul, SP, Brazil), at 373 K for 48 h, and ground in a domestic grinder (MDR3, Cadence, Navegantes, SC, Brazil) at the Laboratory for Environmental Management, Control, and Preservation (LGCPA) of the State University of Maringa (UEM). Finally, the ground material was sieved using a set of sieves mounted on a vibrating table (BT–001, Brix, Piracicaba, Brazil), and the fraction passing a 350 µm mesh was retained. This material is designated SPC. The preparation of the adsorbent is summarised in Figure 2.

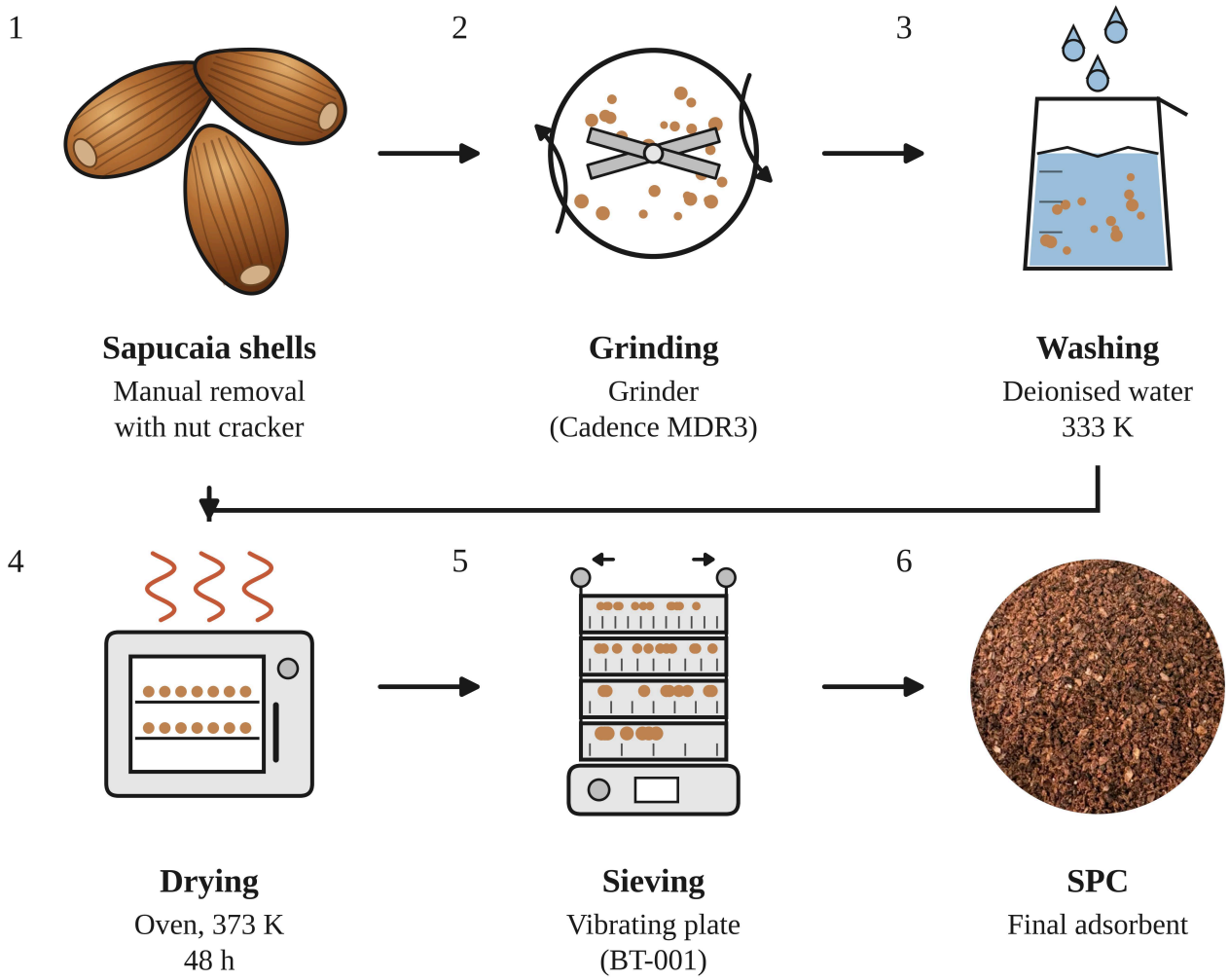


Figure 2. Preparation of the Sapucaia shell powder (SPC) adsorbent. Numbers 1-6 indicate the sequence of the preparation steps.

2.1.3. Characterisation Techniques

To analyse the morphological structure of the SPC surface, scanning electron microscopy analysis (SEM, Quanta 250, FEI Company, Hillsboro, OR, USA) was employed, performed using topographic contrast. The surface charge of the adsorbent was determined using the zeta potential technique (Delsa™ Nano C, Beckman Coulter, Brea, CA, USA), with the pH of the solutions adjusted using 0.1 M HCl and NaOH solutions. Fourier-Transform Infrared Spectroscopy (FTIR, Vertex 70v, Bruker Optik GmbH, Ettlingen, Germany), operating in the 4000–400 cm^{-1} range at room temperature, was employed to identify and define the functional groups present in the material. In addition, X-ray diffraction (XRD, D8 Advance, Bruker AXS GmbH, Karlsruhe, Germany) analysis was performed to characterise the crystalline structure of SPC. Scanning electron microscopy and zeta potential measurements were also performed on SPC after CQN adsorption, using the material recovered from the adsorption tests washed with deionised water and dried prior to analysis.

2.1.4. Adsorption Experiments

All batch adsorption experiments were performed on a temperature-controlled shaker table (TE–4200, Tecnal, Piracicaba, SP, Brazil) at 150 rpm. The experiments were performed in duplicate and the initial concentration was reported for each experiment. First, the SPC dosage (0.01, 0.03, and 0.05 g) was evaluated in contact with 30 mL of

CQN solution at 26.61 mg L^{-1} and 298 K for 24 h. The solution volume was selected to ensure a sufficient sample volume for spectrophotometric analysis after separation of the adsorbent and the initial concentration was adopted from previous studies on the removal of emerging contaminants using agro-industrial residues [39]. After determining the optimal adsorbent dosage, the influence of pH (4, 7, 10 and the natural pH of the solution (≈5.03)) was evaluated using a CQN concentration of 26.05 mg L^{-1} and the same solution volume. Both sets of experiments were conducted at 298 K with a contact time of 24 h.

The kinetic study was carried out to determine the equilibrium time of the adsorption process. The samples were collected over 24 h. The conditions established previously were retained (C_0 = 26.0 mg L^{-1}, V = 30 mL, contact time = 24 h, stirring speed = 150 rpm). The experimental data were fitted to pseudo-first-order, pseudo-second-order, and Elovich kinetic models.

Adsorption–desorption experiments were performed on SPC to evaluate its regeneration performance and the viability of reuse. Tests were conducted under the conditions previously identified as optimal (C_0 = 26.05 mg L^{-1}, V = 30 mL, contact time = 24 h, stirring speed = 150 rpm).

For the adsorption isotherms, the initial concentration was varied from 5 to 150 mg L^{-1}, and the experiments were conducted at the equilibrium contact time of 24 h at three temperatures (288, 293, and 298 K), using 0.03 g of SPC in 30 mL of solution. At the end of each experiment, the samples were filtered through 0.45 µm cellulose acetate membranes (UNIFIL). The initial and final CQN concentrations were both measured using a UV-Vis spectrophotometer (DR 6000, Hach, Loveland, CO, USA) at a wavelength of 343 nm, with the respective standard curves previously prepared from standard solutions (R^2 = 0.9994; Figure S1). The adsorption capacity (q_e) was calculated by Equation (1). Preliminary experiments at 308 and 318 K were also conducted but were excluded from the analysis owing to colour leaching from the lignocellulosic matrix, which interfered with UV-Vis readings at 343 nm, the temperature range was therefore restricted to 288–298 K. To confirm that colour leaching did not affect CQN quantification at the adopted temperatures, adsorbent blanks (SPC in deionised water without CQN, under identical conditions) were run in parallel.

$$q_e = \frac{(C_0 - C_e) \cdot V}{m} \quad (1)$$

where C_0 and C_e are the initial and equilibrium contaminant concentrations (mg L^{-1}), respectively; V is the solution volume (L); and m is the adsorbent mass (g).

Non-linear regression of the kinetic and isotherm models and plotting of the experimental data were performed using OriginPro version 8.5 (OriginLab Corporation, Northampton, MA, USA; https://www.originlab.com).

3. Results and Discussion

3.1. Characterisation

3.1.1. SEM

Through the images presented in Figure 3, analysis of the adsorbent material morphology was carried out.

The images in Figure 3 demonstrate an irregular, heterogeneous morphology, with the presence of several cavities. Such features are characteristic of lignocellulosic adsorbents [40].

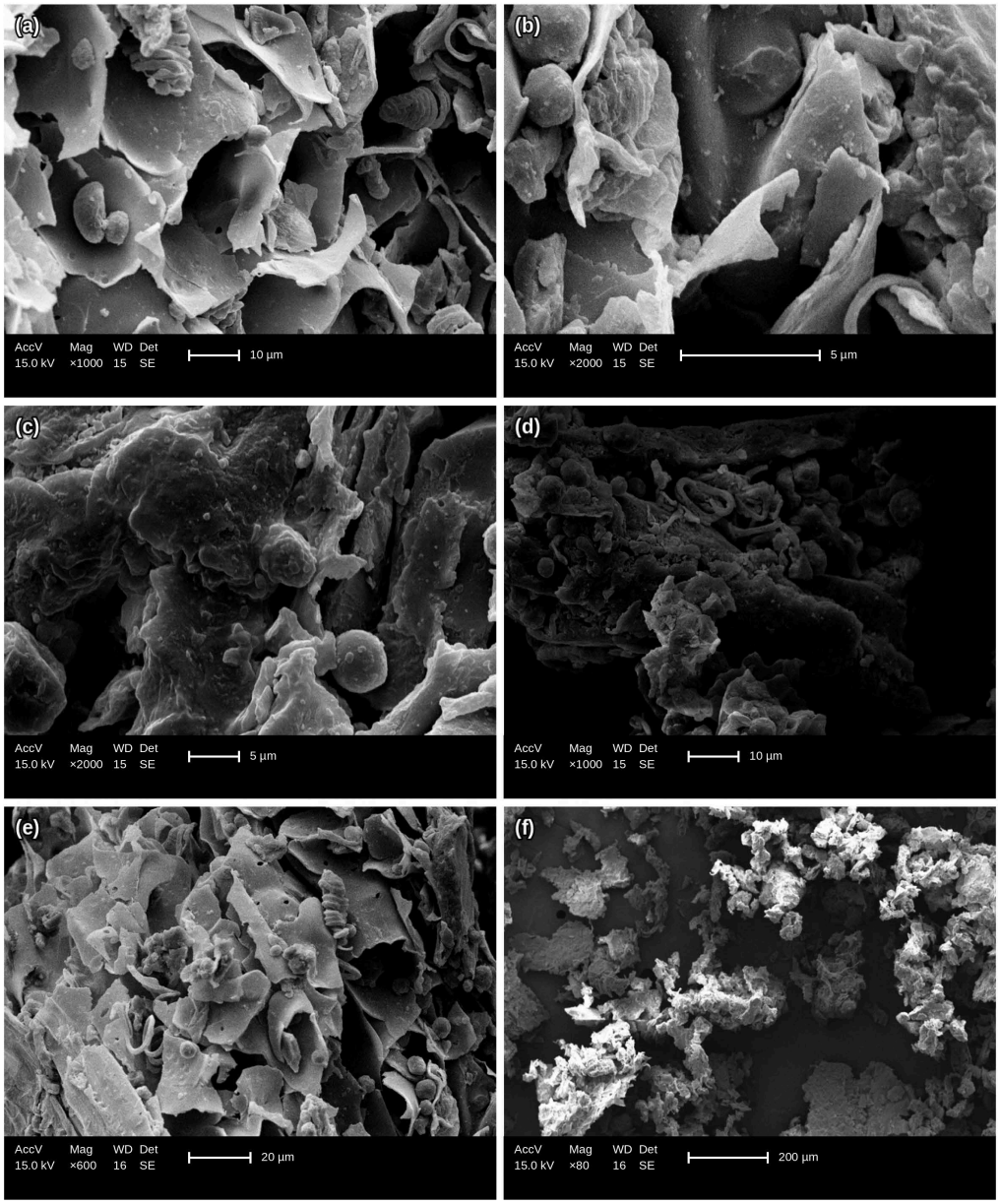


Figure 3. Analysis of scanning electron microscopy on the adsorbent SPC in: (**a**) 1000×; (**b**) 2000×; (**c**) 2000×; (**d**) 1000x; (**e**) 600×; (**f**) 80×.

3.1.2. Zeta Potential

The zeta potential analysis allows knowledge of the surface charges of materials, which are important characteristics for understanding the interaction between adsorbent and adsorbate [41]. Measured at different pH values, the free ions in the solution interact with the adsorbent and as the pH approaches the material's point of zero charge, we have the isoelectric point [32].

According to Figure 4, the results of the zeta Ppotential analysis show a material with a predominantly negative charge and an isoelectric point around pH 2. At pH 6, the material has a charge of −31.75 mV, with charge variation of −0.77 to −59.40 mV at pH values 2 to 12. The negative characteristic of the material is related to lignocellulosic materials, as well as the presence of phenolic and carboxylic groups, known for their deprotonation capacity. Such properties have been found in other lignocellulosic adsorbents previously [26].

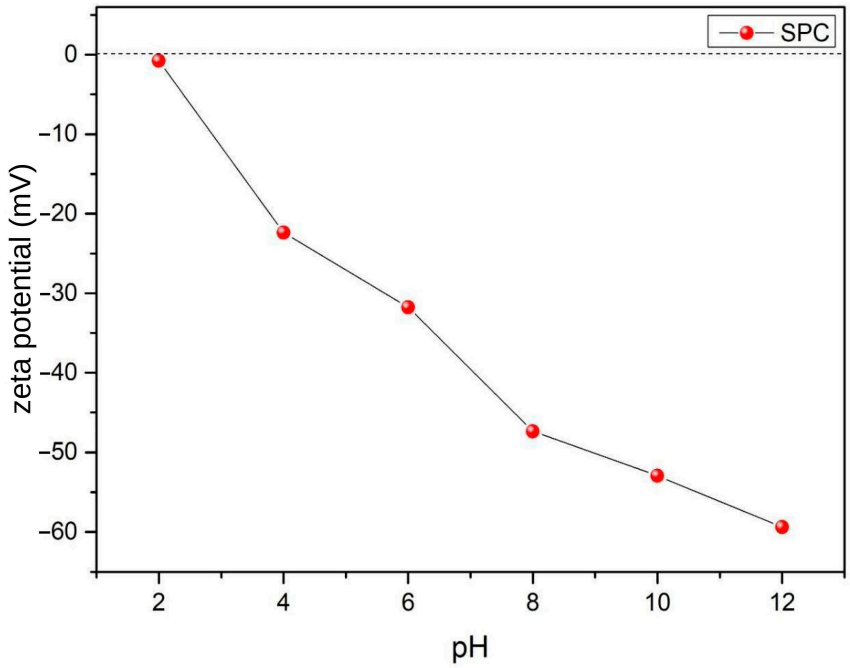


Figure 4. Zeta potential of SPC. The dashed line marks zero zeta potential.

3.1.3. XRD

The image presented in Figure 5 illustrates the characteristic X-ray diffraction (XRD) profile of the SPC adsorbent.

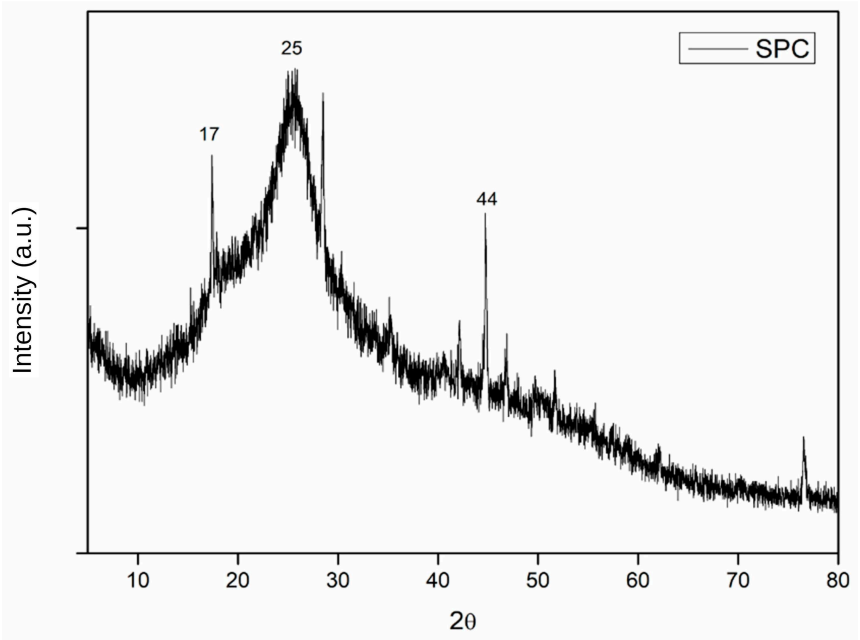


Figure 5. X-ray diffraction (XRD) analysis of SPC.

In the X-ray diffraction pattern shown in Figure 5, it is observed that the material is predominantly amorphous, with more evident crystallinity peaks at 17, 25 and 44°. Such results may be related to the presence of type I cellulose (17 and 25°) [32,42], and to the carbon compounds in the material (25 and 44°) [33,43]. The crystallinity peaks observed may be related to the function of the seed protection material, which provides resistance and hardness to their shells [32].

3.1.4. FTIR

The FTIR analysis allows us to identify the functional groups on the surface of the adsorbent, responsible for the interaction between adsorbent and adsorbate, according to the characteristic spectra of the SPC, shown in Figure 6 [44,45].

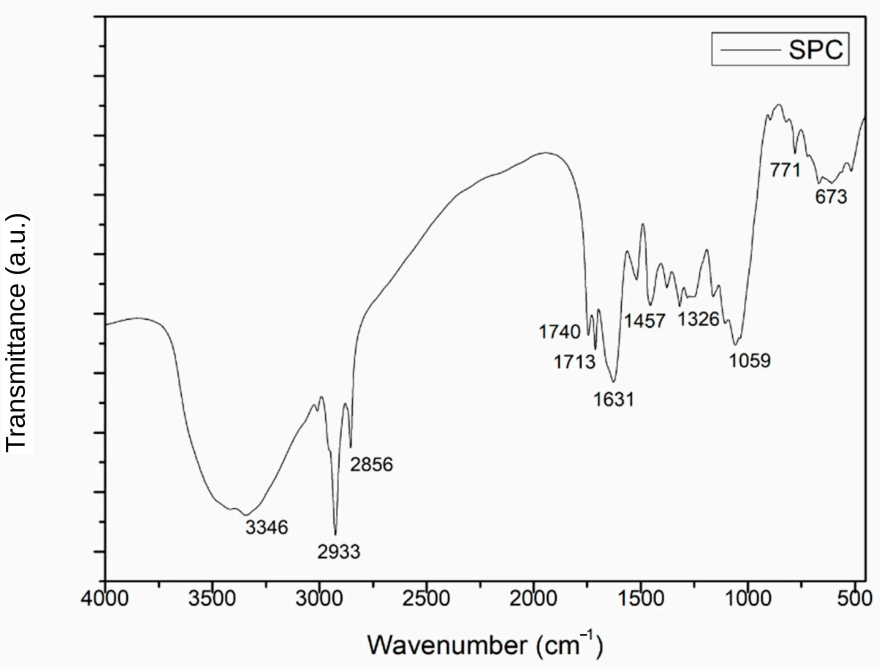


Figure 6. Fourier-Transform Infrared Spectroscopy of SPC.

Observing the FTIR spectrum (Figure 6), it is possible to identify peaks and bands around 3346, which may be related to the –OH group, referring to the hydroxyl of the material, characteristic of cellulose and hemicellulose [46]. In other studies, a broadband at 3500–3200 cm^{-1} was observed for macadamia nutshell, indicating the high hydrophilicity of the residue [47].

The peaks identified at 2933 and 2856 cm^{-1} may be related to the stretching vibrations of the symmetric and asymmetric C-H bonds from cellulose alkyl groups [48]. Also, the peaks at 1740 and 1713 cm^{-1} are reported by the presence of carboxylic groups (-COOH) related to hemicellulose [42] and usually present in fibre materials containing pectin [49]. Also, amide I may be related to the signal indicated by the band at 1631 cm^{-1} [50]. According to Bansal and Goyal (2005) [51], the signals found between 1775 and 1675 cm^{-1} indicate the presence of lactone groups (-OOR) and quinones [43]. Furthermore, the signals found at 1457 cm^{-1}, 1326 cm^{-1} and 1059 cm^{-1} may be related to the presence of the C-H group [52], conjugated C=O bonds and the C-O bond stretching in carboxylic groups and phenols, characteristic of materials rich in tannins, such as the skins of some oilseeds [33,49], and C-N aromatic stretching peaks [53], respectively.

The bending vibration bands which occurred around 670–770 cm^{-1} may be related to the vibrational out-of-plane bending movements of polyphenolic –OH groups; they can also correspond to both the long-chain nonpolar compounds $(CH_2)n$– as well as out-of-plane deformation in substituted phenolic groups. This region can be related to the crystallinity characteristics of cellulose I, β and α [54].

3.2. Influence of Variables on Adsorption

3.2.1. Mass/pH Removal Tests

The effects of adsorbent dosage and solution pH on the adsorption capacity of SPC for CQN were evaluated (Figure 7). Three adsorbent masses were tested: 0.01 g, 0.03 g and 0.05 g at an initial concentration of 26.61 mg L^{-1}. Increasing the adsorbent mass raised the removal from 79% at 0.01 g to 82% at 0.03 g, after which it decreased to 75% at 0.05 g. A mass of 0.03 g was therefore used in the subsequent tests, since it gave a promising rate for adsorption and removal capacity (q_e 21.72 mg g^{-1}).

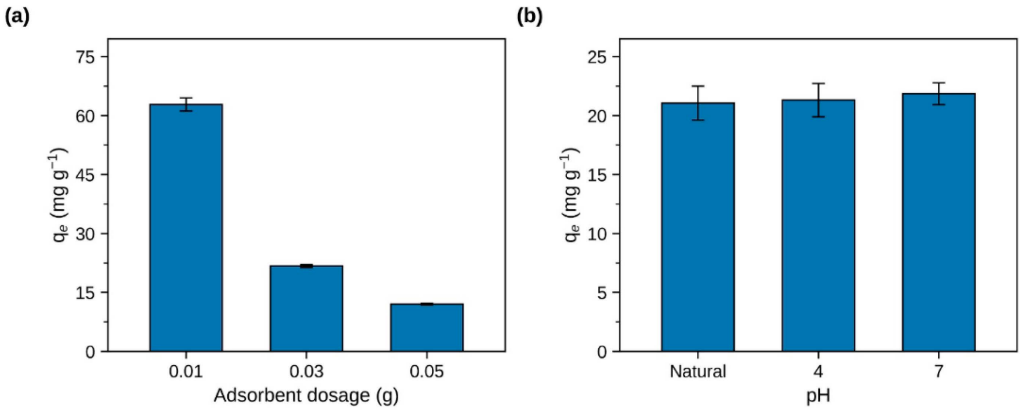


Figure 7. Effect of (**a**) adsorbent dosage and (**b**) solution pH on the adsorption capacity (q_e) of chloroquine (CQN) onto SPC. Conditions: (**a**) V = 30 mL, C_0 = 26.61 mg L^{-1}, and natural pH; (**b**) V = 30 mL, m = 0.03 g, and C_0 = 26.05 mg L^{-1}; both at T = 298 K, 150 rpm and 24 h of contact time.

Because it alters both the charge of the adsorbent surface and the speciation of the functional groups of the contaminant, pH is considered one of the most important control parameters in the adsorption process [54]. The adsorption capacity for CQN was evaluated at pH 4, 7, 10, and at the natural pH of the solution at an initial concentration of 26.05 mg L^{-1}. The highest removal was obtained at pH 7 with 84% (q_e 21.85 mg g^{-1}). The natural pH gave 81% removal (q_e 21.06 mg g^{-1}) and was therefore selected for the subsequent experiments, since the removal efficiency obtained was comparable to that obtained at pH 7, while avoiding the need for pH adjustment.

Adsorption was also evaluated at pH 10; this condition was subsequently excluded from the analysis owing to colour leaching from the lignocellulosic matrix, which interfered with UV-Vis readings at 343 nm. The same phenomenon was observed in the preliminary experiments at elevated temperatures (Section 2.1.4).

3.2.2. Adsorption Kinetics

Kinetic analysis provides essential information for elucidating the adsorption process, such as the evolution of adsorption capacity over time until equilibrium is reached [55]. A kinetic study was performed under the conditions identified above, over a total period of 1440 min (Figure 8). Between 600 and 800 min, minimal variation in adsorption capacity was observed, confirming the attainment of equilibrium. The equilibrium adsorption capacity (q_e) obtained was approximately 17.92 mg g^{-1}; this value represents the maximum chloroquine uptake under the experimental conditions and indicates substantial adsorption potential for this lignocellulosic biosorbent in the treatment of water contaminated with CQN.

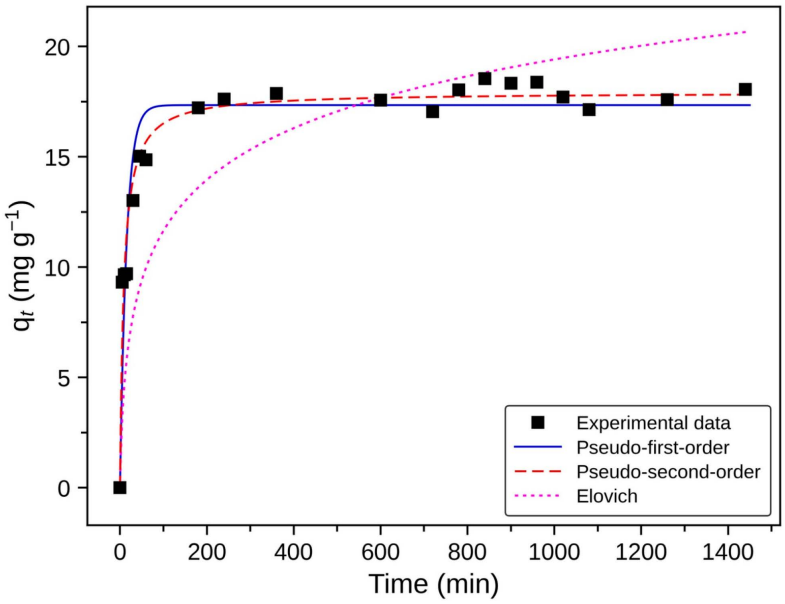


Figure 8. Kinetic data of SPC adsorption onto CQN (C_i = 26.0 mg L^{-1}, SPC concentration = 0.03 g, natural pH, T = 298 K, stirring speed = 150 rpm).

The pseudo-first-order, pseudo-second-order and Elovich models were fitted to the experimental data to characterise the adsorption kinetics. The parameters are presented in Table 1.

Table 1. Parameters of kinetic models fitted for CQN adsorption onto SPC.

Models	Equation	Parameters	SPC
Pseudo-first-order	$q_t = q_e\ (1 - e^{-k_1 t})$	q_e, exp (mg g^{-1}) q_e, calc (mg g^{-1}) k_1 (min^{-1}) R^2 χ^2	17.4289 ± 0.38504 17.43 0.0669 ± 0.00935 0.90919 2.12092
Pseudo-second-order	$q_t = k_2 q_e^2 t/(1 + k_2 q_e t)$	q_e, calc (mg g^{-1}) k_2 (g mg^{-1} min^{-1}) R^2 χ^2	17.92006 ± 0.25767 0.00654 ± 8.18692 × 10^{-4} 0.96565 0.80233
Elovich model	$dq_t/dt = a\ e^{-bq_t}$	a (mg g^{-1} min^{-1}) b (g mg^{-1}) R^2 χ^2	1 ± 0.70921 0.29279 ± 0.05349 0.48016 12.14108

The pseudo-second-order model gave the best statistical fit, with the highest correlation coefficient (R^2 = 0.96565) and the lowest chi-squared value (χ^2 = 0.80233), a measure of the residual error. The Elovich model gave the poorest fit (R^2 = 0.48016). These results suggest that the chloroquine adsorption mechanism may involve chemisorption, in which valence forces arising from the sharing or exchange of electrons between the adsorbent and the adsorbate may operate [56].

The pseudo-second-order rate constant (k_2) describes the rate at which adsorption occurs. In this study, the k_2 was 0.00654 g mg^{-1} min^{-1}, higher than the values reported for chloroquine removal using a natural adsorbent (≤0.00388 g mg^{-1} min^{-1}) [57].

Recent studies indicate that chloroquine adsorption onto various natural materials follows a consistent trend, with the pseudo-second-order model giving the best fit ($R^2 > 0.99$), which suggests a chemisorption-controlled mechanism [2,24,58,59].

The kinetic data were fitted to the Weber–Morris [60] intraparticle diffusion model ($q_t = k\text{id}\cdot t^{1/2} + C$, where kid is the intraparticle diffusion rate constant and C is the intercept related to the boundary layer thickness). Under this model, intraparticle diffusion is the sole rate-limiting step only if the plot of q_t versus $t^{1/2}$ passes through the origin. The fitted parameters for each linear segment are summarised in Table 2. Figure 9 shows three zones, each governed by a distinct mass-transfer mechanism.

Table 2. Weber–Morris intraparticle diffusion model parameters for CQN adsorption onto SPC.

Phase	K_{id} (mg g^{-1} min$^{-1/2}$)	C (mg g^{-1})	R^2
1st (0–80 min)	1.7917	9.4429	0.9926
2nd (80–600 min)	0.1121	15.9715	0.9845
3rd (600–1440 min)	0.0089	17.6825	0.8924

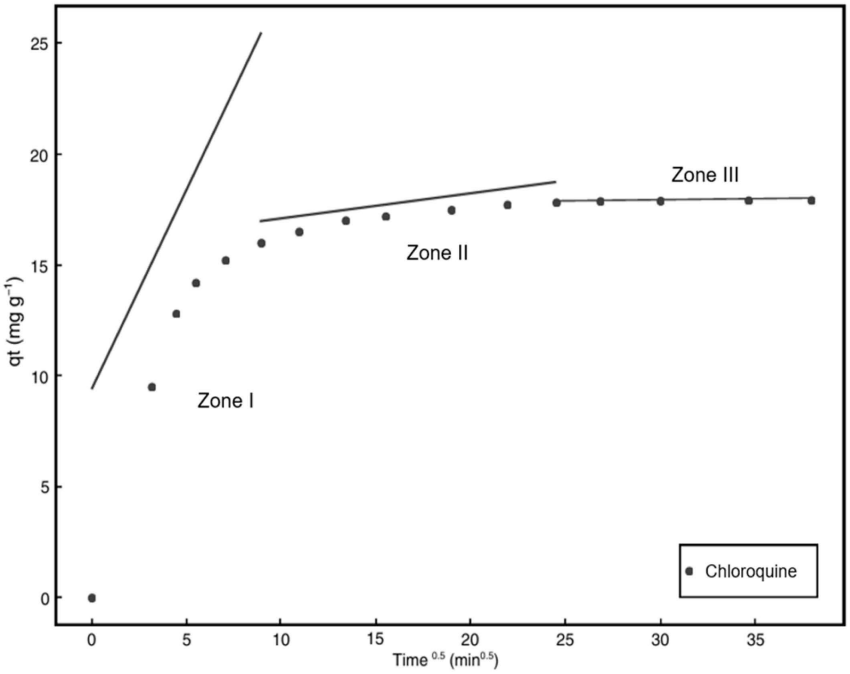


Figure 9. Intraparticle diffusion of CQN onto SPC fitted to the Weber–Morris model, showing the three mass-transfer stages (C_0 = 26.0 mg L^{-1}, m = 0.03 g, V = 30 mL, natural pH, T = 298 K, stirring speed 150 rpm).

The first phase (0–80 min) showed strong linearity ($R_1^2 = 0.9926$) and the highest kid value of the three stages, indicating rapid external surface adsorption driven by the large initial concentration gradient between the bulk solution and the biosorbent surface. This behaviour reflects a high initial affinity between CQN molecules and the available active sites on the SPC surface. A study using cobalt-modified mesoporous silica for chloroquine removal reported a comparable pattern of rapid initial diffusion with low resistance and non-zero intercepts [61].

The second phase (80–600 min) retained good linearity ($R_2^2 = 0.9845$), albeit with a lower kid value than the first, which reflects the gradual diffusion of CQN molecules into the pores of the SPC matrix. The decrease in diffusion rate is attributable to the increasing resistance encountered as the adsorbate migrates from the external surface into the interior of the biosorbent particles. A similar trend was found in a previous study, in which the

adsorption rate decreased progressively as chloroquine penetrated the pores of activated carbon [58].

The third phase (600–1440 min) corresponds to the equilibrium stage, with weaker but still acceptable linearity (R_3^2 = 0.8924) and the smallest *k*id value, indicating gradual saturation of the remaining active sites. The applicability of the Weber–Morris model is supported by the correlation obtained in all three phases (R^2 > 0.89); the non-zero intercept values (C > 0) indicate, however, that intraparticle diffusion is not the sole rate-controlling step and that boundary layer resistance also contributes to the overall mass-transfer process [24,26,60].

3.2.3. Adsorption Isotherms

An equilibrium isotherm describes the relationship between the adsorption capacity of the material (q_e) and the equilibrium solute concentration in an aqueous solution (C_e) under constant-temperature conditions [62]. Isotherms were determined over a range of initial adsorbate concentrations (5–150 mg L^{-1}) at three temperatures (288, 293 and 298 K), as shown in Figure 10. The experimental data were fitted to the Langmuir, Freundlich, Temkin and Sips models and the corresponding parameters are given in Table 3.

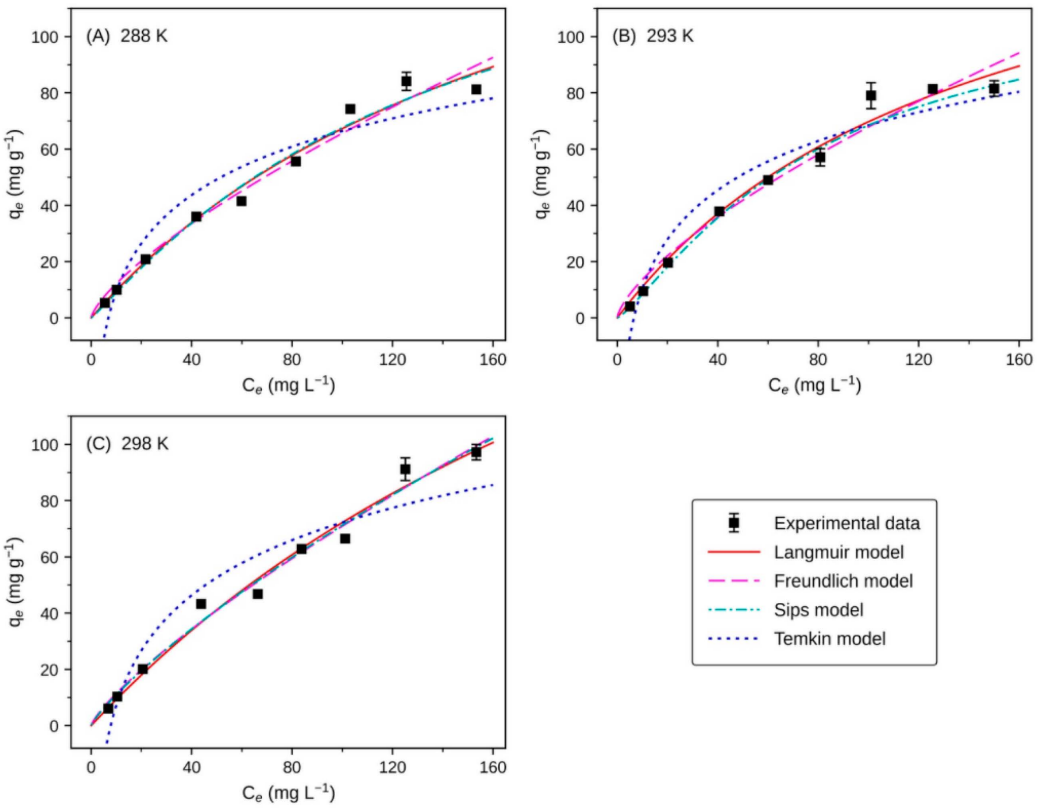


Figure 10. CQN adsorption on SPC isotherms at temperatures of 288 K (A), 293 K (**B**) and 298 K (**C**) (C_0 = 5–150 mg L^{-1}, m = 0.03 g, V = 30 mL, natural pH, stirring speed 150 rpm, 24 h of contact time).

Preliminary tests at 308 K and 318 K showed colour leaching from the lignocellulosic matrix present in the Sapucaia shell, which led to interference in the spectrophotometer reading and compromised the accuracy of the results. The same effect has been reported previously as high temperatures increased the solubility and extraction rate of phenolic compounds and tannins from lignocellulosic matrices, which promotes their migration to the aqueous phase [63–65]. The temperature range was therefore restricted to 288–298 K.

Table 3. Parameters of adsorption isotherm models fitted to the experimental data at 288, 293 and 298 K.

Model	Equation	Parameter	288 K	293 K	298 K
Langmuir	$q_e = q_{max}\ K_L\ C_e/(1 + K_L\ C_e)$	q_{max} (mg g^{-1})	196.3934 ± 42.20989	170.02937 ± 28.32571	293.69488 ± 88.92429
		K_L (L mg^{-1})	0.00521 ± 0.00173	0.00695 ± 0.00196	0.00326 ± 0.00134
		R^2	0.98003	0.982	0.98258
		R^2_{adj}	0.9734	0.9760	0.9768
		χ^2	2.19	2.70	2.96
		AIC	29.05	28.48	29.52
Freundlich	$q_e = k_F C_e^{1/n}$	K_F	2.24657 ± 0.73621	2.72516 ± 0.93771	1.84149 ± 0.51502
		n	1.36483 ± 0.13257	1.43248 ± 0.15414	1.26133 ± 0.09631
		R^2	0.9733	0.96813	0.98382
		R^2_{adj}	0.9644	0.9575	0.9784
		χ^2	3.79	6.66	3.28
		AIC	31.66	33.62	28.86
Temkin	$q_e = (RT/b_T)\ \ln(K_T\ C_e)$	K_T (L mg^{-1})	0.14497 ± 0.03639	0.15117 ± 0.03277	0.12837 ± 0.03037
		b_T (mg g^{-1})	24.83044 ± 2.9172	25.23308 ± 2.53252	28.31518 ± 3.27763
		R^2	0.91189	0.93413	0.91425
		R^2_{adj}	0.8825	0.9122	0.8857
		χ^2	31.21	25.23	37.10
		AIC	42.41	40.16	43.87
Sips	$q_e = k_{sCe}{}^{ns}/(1 + a_{s\ Ce}{}^{ns})$	q_{max} (mg g^{-1})	168.16289 ± 87.79373	121.11672 ± 31.25351	989.19219 ± 4135.850
		K_s	0.00692 ± 0.00645	0.01235 ± 0.00549	4.77614×10^{-4} ± 0.00295
		n	1.0783 ± 0.28019	1.24208 ± 0.26331	0.84029 ± 0.2283
		R^2	0.98032	0.98464	0.98397
		R^2_{adj}	0.9685	0.9754	0.9744
		χ^2	2.35	1.73	3.01
		AIC	30.92	29.05	30.78

Model performance was evaluated using R^2, adjusted R^2 (R^2_{adj}), χ^2, and the Akaike information criterion (AIC). Adjusted R^2 and AIC were considered alongside R^2 to account for model complexity and allow a fairer comparison between models [66].

The Sips model was initially considered but proved over-parameterised for the data. At 298 K the standard error of q_{max} exceeded the fitted value. Although its R^2 was comparable to those of the models with two parameters, both R^2_{adj} and AIC were less favourable at all three temperatures, suggesting that the additional parameter was not supported by the data. The model was therefore excluded from further analysis.

Among the remaining models, the Langmuir and Freundlich models gave comparable fits, with R^2_{adj} values of 0.957–0.978 and χ^2 values of 2.2–6.7. The Freundlich exponent remained between 1.26 and 1.43 across all temperatures and the 1/n values between 0.70 and 0.79, which indicates favourable adsorption; the distance from unity also indicates that adsorption sites are not all equivalent, consistent with the lignocellulosic nature of SPC as well as with the irregular surface seen in the SEM images. In contrast, Temkin gave a weaker fit at all three temperatures, with R^2_{adj} values of 0.883–0.912, considerably higher χ^2 values, and the least favourable AIC. The system therefore appears not to follow the Temkin assumption of a uniform decrease in the heat of adsorption with surface coverage.

The Langmuir-fitted q_{max} obtained in this study was compared with values reported in the literature for chloroquine removal using agro-industrial waste-based adsorbents, as summarised in Table 4. As the values compiled in Table 4 correspond to Langmuir-fitted parameters, they represent model extrapolations rather than directly measured capacities. In the present work, the maximum experimental adsorption capacity was 97.26 mg g^{-1}, obtained at 298 K for an equilibrium concentration of 56.14 mg L^{-1}. These results underline the potential of the unmodified Sapucaia shell as a competitive lignocellulosic biosorbent for chloroquine removal.

Table 4. Comparison of CQN adsorption capacities for different agro-industrial waste-based adsorbents.

Adsorbent	q_{max} (mg g^{-1})	T (K)	Reference
Açaí activated biochar (CAA)	40.31	298	Santos et al., 2023 [58]
Sunflower seed husks (SSH)	168.09	298	Ferreira et al., 2024 [57]
Cassava biochar	39.00	318	Gonçalves et al., 2024 [25]
Black soybean hulls	70.99	298	Januário et al., 2024 [39]
Coconut shell activated carbon	150.00	298	Oreofe et al., 2024 [67]
Hibiscus sabdariffa biochar	161.29	303	Bankole et al., 2022 [68]
SPC	293.69 *	298	This study

* Langmuir q_{max}.

3.2.4. Thermodynamic Parameters

The feasibility of the adsorptive process as a function of temperature can be evaluated through thermodynamic parameters [62]. The Gibbs free energy (ΔG°), enthalpy (ΔH°), and entropy (ΔS°) of chloroquine adsorption onto Sapucaia shell were calculated from the Langmuir constant [69].

The ΔG° was negative (−3.46, −4.31, and −5.15 kJ mol^{-1}) at all three temperatures (288, 293, and 298 K), which indicates a spontaneous and favourable process, without the necessity for external energy input [70].

The enthalpy value (ΔH°) was positive (+45.82 kJ mol^{-1}), which confirms that the process is endothermic. ΔH° also exceeded the range generally reported for physical adsorption (2–40 kJ mol^{-1}), which indicates that the process is not purely physical. These results indicate a mixed mechanism involving specific interactions with the functional groups of the lignocellulosic matrix, such as hydrogen bonding and π–π interactions, which contribute significantly to chloroquine retention [71].

The entropy value (ΔS°) was positive at 169.31 J mol^{-1} K^{-1}, which indicates an increase in randomness at the solid–liquid interface. This result may be attributed to changes such as the reorganisation of water molecules around the functional groups of the adsorbent and conformational changes in the lignocellulosic matrix [24,68].

3.2.5. Effects of Ionic Strength

The interactions between adsorbent and adsorbate may be affected by an increase in the concentration of other ions dissolved in the aqueous matrix, which compete with the pollutant for the active sites available on the adsorbent surface [72]. Figure 11 shows the effect of sodium chloride (NaCl) and calcium chloride ($CaCl_2$) at 0.1 and 0.3 mol L^{-1} at an initial concentration of 26.0 mg L^{-1}.

Ionic strength modulates the electrostatic interactions that govern the adsorption process. Both electrolytes reduced the adsorption of CQN onto SPC. With NaCl, the adsorption capacity decreased from 13.73 mg g^{-1} (53% removal) at 0.1 mol L^{-1} to 9.78 mg g^{-1} (38% removal) at 0.3 mol L^{-1}. With $CaCl_2$, the capacity decreased from 8.78 mg g^{-1} (34% removal) to 6.50 mg g^{-1} (25% removal) over the same range.

At the same molar concentration, $CaCl_2$ had a stronger suppressive effect than NaCl. This behaviour indicates that the electrolyte cations compete with protonated chloroquine for the negatively charged sites on the SPC surface, with divalent Ca^{2+} competing more effectively than monovalent Na^+ [21,61]. Higher ionic strength also compresses the electrical double layer at the solid–solution interface, which weakens the electrostatic attraction between the surface and the adsorbate. These results are consistent with the negative surface charge of SPC observed from the zeta potential measurements and with the neutralisation of this charge after adsorption (Section 3.3.2). These results suggest that protonated CQN

species occupy negatively charged surface sites, which are also involved in the competition with electrolyte cations.

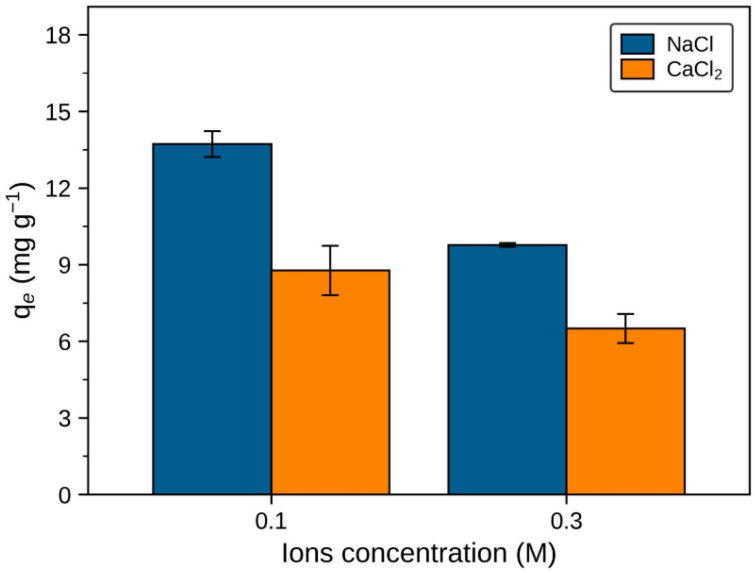


Figure 11. Effect of ionic strength on the adsorption of CQN onto SPC in the presence of NaCl and $CaCl_2$ at 0.1 and 0.3 mol L^{-1} (C_0 = 26.0 mg L^{-1}, m = 0.03 g, V = 30 mL, natural pH, T = 298 K, 150 rpm, 24 h of contact time).

3.2.6. Regeneration Studies

Because effluent treatment operates on an industrial scale, it requires adsorbents that can be reused, thereby minimising waste generation and reducing operational costs [73]. Desorption was first tested with four different solvents: distilled water, 0.1 M HCl, 0.1 M NaOH, and analytical-grade ethyl alcohol. As shown in Figure 12, although distilled water gave the lowest desorption of the four eluents, it was selected as the regeneration medium due to its environmental compatibility and because it avoids the secondary contamination risks posed by chemical eluents. This choice prioritises practical applicability and green chemistry principles over maximum desorption efficiency, consistent with the sustainability-oriented design of this study.

Four consecutive adsorption–desorption cycles of 24 h each were performed at an initial concentration of 26.05 mg L^{-1}. Over the four cycles, the adsorption capacity decreased from 21.27 mg g^{-1} in the first cycle to 13.79 mg g^{-1}, a retention of approximately 65% of the initial capacity. This progressive reduction is consistent with previous findings, in which approximately 70% was retained after five cycles for biochar [26].

To assess whether this behaviour was maintained at higher loading, an additional experiment was carried out at an initial concentration of 150 mg L^{-1} (Figure 12b). The adsorption capacity fell from 87.6 mg g^{-1} to 34.5 mg g^{-1}, a retention of 39%.

These results suggest that the reuse of SPC depends on the adsorbate loading, considering that at higher concentrations the amount of CQN released by water during desorption may be insufficient to restore the adsorption sites for the next cycle [74], and that the residual adsorbate progressively limits the capacity of the subsequent cycles.

Over three cycles, the retention obtained at 26.05 mg L^{-1} was 89%, higher than the values reported for cobalt-modified mesoporous silica, for which capacity fell by more than 35% [61], and for plant-based fibres, which lost more than 40% even under chemical regeneration [75]. At 150 mg L^{-1}, retention under the same number of cycles was lower than both, which indicates that alternative regeneration approaches may be required at higher adsorbate concentrations.

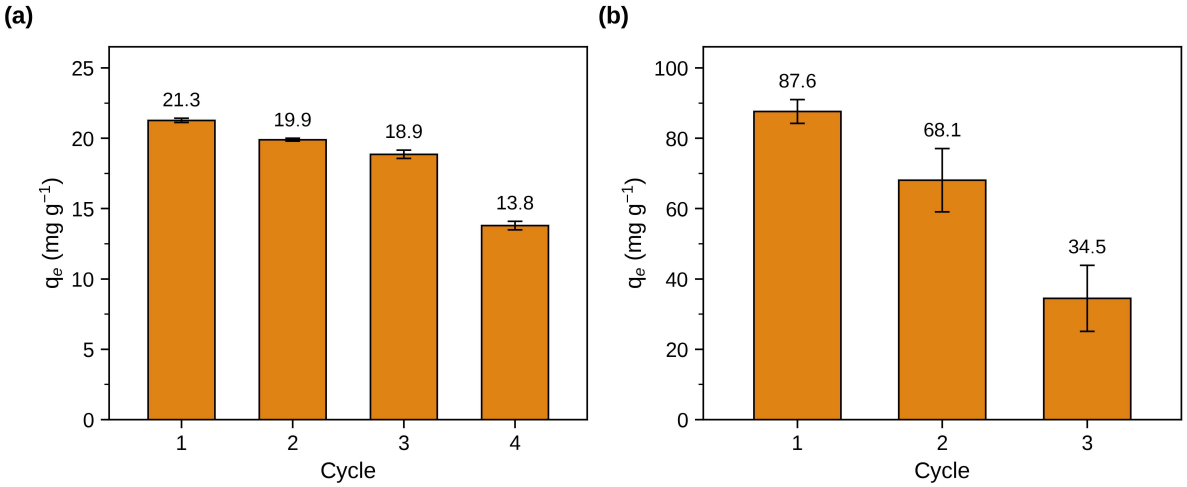


Figure 12. Reuse of SPC over consecutive adsorption–desorption cycles using distilled water as the desorbing agent at initial concentrations of (**a**) 26.05 mg L^{-1} and (**b**) 150 mg L^{-1}. Conditions: m = 0.03 g, V = 30 mL, natural pH, T = 298 K, 150 rpm, 24 h of contact time per cycle.

3.3. Post-Adsorption Characterisation

To support the proposed adsorption mechanisms, the SPC was characterised after CQN adsorption and compared with the original material. The samples were recovered after contact with CQN solution under the conditions established in Section 2.1.4, washed with deionised water to remove non-adsorbed CQN and dried at room temperature.

3.3.1. SEM

Figure 13 shows scanning electron micrographs of SPC before and after CQN adsorption, at equivalent fields of view. The original material (Figure 13a,c) shows an irregular and heterogeneous morphology with several cavities as described in Section 3.1.1, characteristic of lignocellulosic adsorbents.

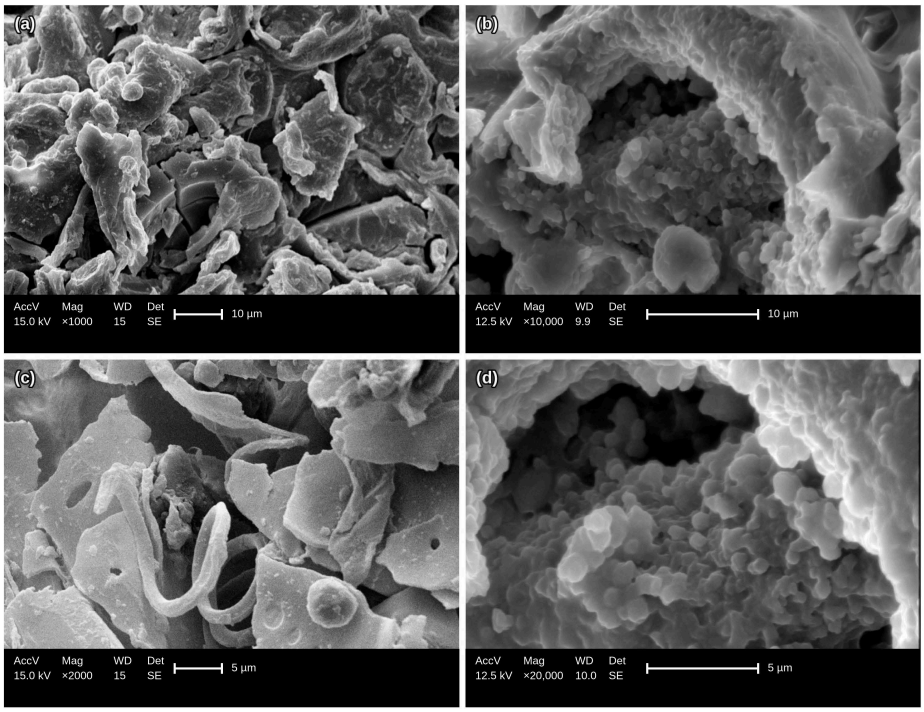


Figure 13. Scanning electron micrographs of SPC before and after CQN adsorption: (**a**) original SPC, 1000×; (**b**) post-adsorption SPC, 10,000×; (**c**) original SPC, 2000×; (**d**) post-adsorption SPC, 20,000×.

After adsorption (Figure 13b,d), the cavities appear largely occupied and the surface less heterogeneous. These changes are consistent with observations reported for other seed-shell biosorbents. In apricot seed shells, the surface micropores of the raw material were absent after dye uptake, which the authors attributed to occupation by the adsorbed molecules [76]. Similarly, in oak acorn pericarp, the surface became less rough and less heterogeneous after adsorption, which the authors attributed to partial blocking of the pores [77].

3.3.2. Zeta Potential

Figure 14 compares the zeta potential of SPC before and after adsorption as a function of pH. For the original material, the zeta potential became increasingly negative with pH, from −2 mV at pH 2 to −54 mV at pH 10, with an isoelectric point close to pH 2. After adsorption, a significant change can be observed, as the zeta potential remained between −4 and 0 mV across the whole range; at pH 6, where the original material gave −33 mV, the value fell to −3 mV.

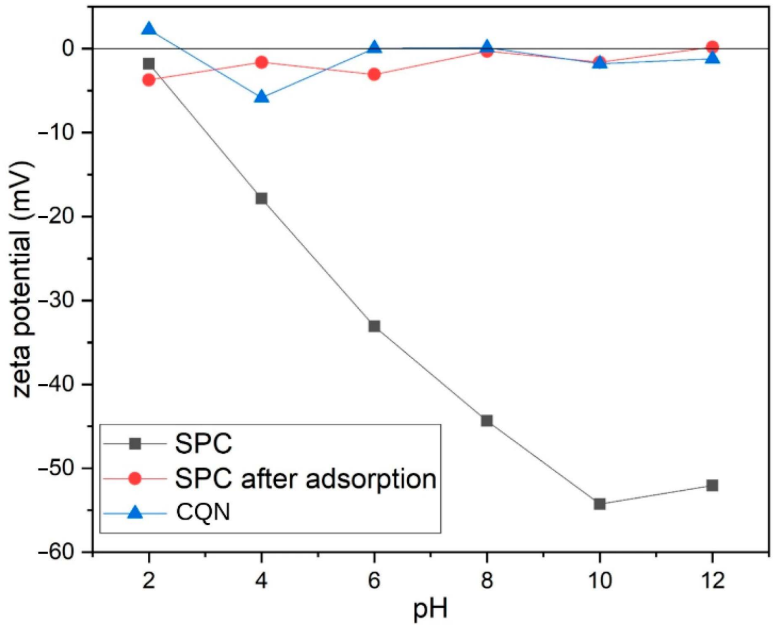


Figure 14. Zeta potential as a function of pH for SPC before adsorption, SPC after CQN adsorption and CQN alone.

The change in surface charge after adsorption suggests that positively charged chloroquine species were retained on the negatively charged surface, which supports the contribution of electrostatic attraction to the adsorption process. Sun et al. [59] reported the same behaviour for chloroquine phosphate on Fe/Mg-modified rape straw biochar, in which the increase in adsorption capacity with pH was attributed to the interaction between the negatively charged adsorbent and the cationic adsorbate.

The similarity between the post-adsorption profile and that of CQN alone further suggests that CQN coats the SPC surface after adsorption. These results are also consistent with the ionic strength effects discussed in Section 3.2.5, where the reduced adsorption observed in the presence of Na^+ and Ca^{2+} suggests competition for the same negatively charged sites.

3.4. Adsorption Mechanism

A multi-mechanistic process involving physical diffusion and surface interactions appears to be responsible for the adsorption process of chloroquine onto the Sapucaia

biosorbent (Figure 15), supported by the structural, kinetic, and surface chemistry analyses performed in this study.

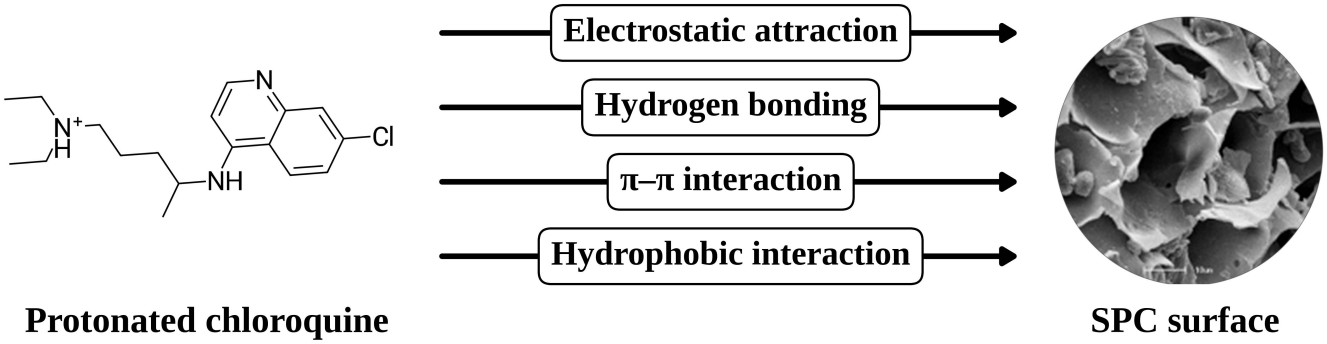


Figure 15. Possible interaction mechanisms between SPC and CQN.

Through zeta potential analysis, it was possible to verify a negative surface charge (−31.75 mV at pH 6), with an isoelectric point around pH 2, which contributes to the relationship with positively charged CQN molecules present in the pH range of natural and treated waters (pH 5–7), since chloroquine has a pK_a of 10.32. Under these conditions the electrostatic interaction between adsorbate and adsorbent is attractive, favouring the approach of CQN molecules to the surface. This is supported by the zeta potential after adsorption (Figure 14), in which the surface charge approached neutrality across the entire pH range. The electrostatic attraction acts in combination with additional interactions, including hydrogen bonding with the phenolic and carboxylic groups of the lignocellulosic matrix, π–π interactions and hydrophobic interactions. The phosphate counter-ions released upon dissociation are not expected to contribute to the mechanism, since they are anionic and are therefore repelled by the negatively charged SPC surface. The Sapucaia FTIR spectrum showed functional groups capable of forming strong hydrogen bonds with the nitrogen and oxygen atoms present in chloroquine molecules, such as carboxyl (–COOH), phenolic (–OH), lactone, and amide. Furthermore, the aromatic structure of chloroquine and the aromatic components derived from Sapucaia lignin allow the formation of π–π stacking interactions. The pseudo-second-order model provided the best fit to the kinetic data (R^2 = 0.9656). However, this result alone does not establish the nature of the adsorption interaction, as the model can also arise at low adsorbate concentrations regardless of the underlying mechanism [78]. In addition, the usual fitting approach tends to favour the pseudo-second-order model over the pseudo-first-order model [79].

Furthermore, the Weber–Morris intraparticle diffusion model demonstrated three distinct phases, showing the gradual filling of the active adsorption sites. Since the graph does not intersect the origin ($C > 0$), it can be inferred that the intraparticle diffusion mechanism is not the only limiting factor in the mass transfer process.

The thermodynamic parameters indicate an endothermic process (ΔH° = +45.82 kJ mol^{-1}) accompanied by a substantial increase in entropy (ΔS° = +169.31 J mol^{-1} K^{-1}). At 298 K, the entropic contribution ($T\Delta S^\circ$ = 50.45 kJ mol^{-1}) exceeds the enthalpic term, suggesting that the negative ΔG° is largely driven by the favourable entropy change. This behaviour may be associated with the release of structured water from the hydration shells of both the adsorbate and the adsorbent surface during adsorption. Although this desolvation process requires energy, the resulting increase in disorder contributes favourably to the overall free energy change. This interpretation is also consistent with the regeneration behaviour, as distilled water alone was able to recover part of the adsorbed CQN over consecutive cycles. Such behaviour is more consistent with reversible interactions than with strong covalent

bonds, which would generally be expected to require more aggressive eluents, such as acidic, alkaline or organic solutions for desorption.

The XRD and SEM image analyses suggest a heterogeneous and irregular matrix, facilitating multiple interactions across internal and external surfaces.

Ionic strength tests corroborate the presence of electrostatic interactions, as both NaCl and $CaCl_2$ reduced the adsorption capacity, with the divalent Ca^{2+} competing more effectively than the monovalent Na^{+}.

Overall, based on the results obtained, it is possible to conclude that the adsorption of CQN onto SPC is governed by physical interactions, with electrostatic attraction between the protonated chloroquine and the negatively charged surface acting in combination with hydrogen bonding between the amino groups of chloroquine and the hydroxyl and carboxyl groups of cellulose and lignin and with π–π interactions between the aromatic rings. The adsorption capacities obtained, achieved without any chemical or thermal treatment of the material, are consistent with the presence of several active functional groups of differing interaction energies.

4. Conclusions

Natural materials with adsorbent capacity for contaminants in aquatic environments have been presented as an excellent alternative for the recovery of waste that would initially be discarded in the quest for decontamination of different water sources. Thus, Sapucaia shell powder (SPC) has proven to be an efficient, sustainable, low-cost and abundant biosorbent for the removal of the drug chloroquine (CQN).

The adsorption isotherms were well described by the Langmuir and Freundlich models at all three temperatures, and the highest experimental adsorption capacity obtained was 97.26 mg g^{-1} at 298 K, consistent with an endothermic process favoured by higher temperatures. Electrostatic attraction between the protonated chloroquine and the negatively charged SPC surface, supported by zeta potential measurements after adsorption, appears to act together with hydrogen bonding, π–π and hydrophobic interactions. Using water alone, SPC retained approximately 65% of its initial capacity after four cycles at 26.05 mg L^{-1}, with lower retention at higher adsorbate loadings.

Finally, the results obtained in this study reveal the potential of Sapucaia shell as a natural adsorbent suitable for removing chloroquine from water, while also being sustainable and economically advantageous. As this is the first study exploring the adsorbent potential of Sapucaia shell, future research addressing possible modifications to the surface of the adsorbent, its application in real effluents and complex matrices, and its performance under competitive conditions may further enrich its use and increase its scalability.

Supplementary Materials: The following supporting information can be downloaded at https://www.mdpi.com/article/10.3390/pr14193050/s1, Figure S1: Calibration curve for CQN quantification at 343 nm.

Author Contributions: Conceptualisation, M.F.R. and R.G.G.; methodology, M.F.R., G.A.V.M.-G., J.V.B. and F.B.B.; software, M.F.R. and A.C.R.; validation, M.F.R. and R.G.G.; formal analysis, M.F.R. and A.C.R.; investigation, M.F.R. and G.A.V.M.-G.; resources, R.B. and L.N.; data curation, M.F.R., G.A.V.M.-G. and A.C.R.; writing—original draft preparation, M.F.R., G.A.V.M.-G. and R.G.G.; writing—review and editing, M.F.R., G.A.V.M.-G. and R.G.G.; visualisation, M.F.R. and R.G.G.; supervision, R.B. and R.G.G.; project administration, R.B. and R.G.G.; funding acquisition, R.B. All authors have read and agreed to the published version of the manuscript.

Funding: This work was supported by the Higher Education Personnel Improvement Coordination (CAPES), Financing Code 001.

Data Availability Statement: Dataset available upon request to the authors. Upon request, the authors will provide the raw data on which the conclusions of this article are based.

Acknowledgments: The authors would like to thank the Research Support Centers Complex (COMCAP) of the State University of Maringa (UEM) for the characterisation analysis.

Conflicts of Interest: The authors declare no conflicts of interest.

References

1. Anastopoulos, I.; Bhatnagar, A.; Hameed, B.H.; Ok, Y.S.; Omirou, M. A Review on Waste-Derived Adsorbents from Sugar Industry for Pollutant Removal in Water and Wastewater. *J. Mol. Liq.* **2017**, *240*, 179–188. [CrossRef]
2. Dada, A.O.; Inyinbor, A.A.; Bello, O.S.; Tokula, B.E. Novel Plantain Peel Activated Carbon–Supported Zinc Oxide Nanocomposites (PPAC-ZnO-NC) for Adsorption of Chloroquine Synthetic Pharmaceutical Used for COVID-19 Treatment. *Biomass Convers. Biorefin.* **2023**, *13*, 9181–9193. [CrossRef]
3. Coatney, G.R. Pitfalls in a Discovery_ the Chronicle of Chloroquine. *Am. J. Trop. Med. Hyg.* **1963**, *12*, 121–128. [CrossRef]
4. White, N.J.; Watson, J.A.; Hoglund, R.M.; Chan, X.H.S.; Cheah, P.Y.; Tarning, J. COVID-19 Prevention and Treatment: A Critical Analysis of Chloroquine and Hydroxychloroquine Clinical Pharmacology. *PLoS Med.* **2020**, *17*, e1003252. [CrossRef]
5. Magagnoli, J.; Narendran, S.; Pereira, F.; Cummings, T.H.; Hardin, J.W.; Sutton, S.S.; Ambati, J. Outcomes of Hydroxychloroquine Usage in United States Veterans Hospitalized with COVID-19. *Med* **2020**, *1*, 114–127.e3. [CrossRef]
6. Lapostolle, F.; Vianu, I.; De Stefano, C.; Goix, L.; Petrovic, T.; Adnet, F. COVID-19 Epidemic: Chloroquine, a French Obsession? *LA Presse Médicale Open* **2021**, *2*, 100007. [CrossRef]
7. Lagier, J.-C.; Million, M.; Gautret, P.; Colson, P.; Cortaredona, S.; Giraud-Gatineau, A.; Honoré, S.; Gaubert, J.-Y.; Fournier, P.-E.; Tissot-Dupont, H.; et al. Outcomes of 3,737 COVID-19 Patients Treated with Hydroxychloroquine/Azithromycin and Other Regimens in Marseille, France: A Retrospective Analysis. *Travel Med. Infect. Dis.* **2020**, *36*, 101791. [CrossRef]
8. Khadka, S.; Yuchi, A.; Shrestha, D.B.; Budhathoki, P.; Al-Subari, S.M.M.; Ziad Alhouzani, T.M.; Anwar Butt, I. Repurposing Drugs for COVID-19: An Approach for Treatment in the Pandemic. *Altern. Ther. Health Med.* **2020**, *26*, 100–107.
9. Chatterjee, T.; Muhkopadhyay, A.; Khan, K.A.; Giri, A.K. Comparative Mutagenic and Genotoxic Effects of Three Antimalarial Drugs, Chloroquine, Primaquine and Amodiaquine. *Mutagenesis* **1998**, *13*, 619–624. [CrossRef]
10. Perez, J.; Roustit, M.; Lepelley, M.; Revol, B.; Cracowski, J.-L.; Khouri, C. Reported Adverse Drug Reactions Associated with the Use of Hydroxychloroquine and Chloroquine During the COVID-19 Pandemic. *Ann. Intern. Med.* **2021**, *174*, 878–880. [CrossRef]
11. Juurlink, D.N. Safety Considerations with Chloroquine, Hydroxychloroquine and Azithromycin in the Management of SARS-CoV-2 Infection. *Can. Med. Assoc. J.* **2020**, *192*, E450–E453. [CrossRef]
12. Belayneh, A. Off-Label Use of Chloroquine and Hydroxychloroquine for COVID-19 Treatment in Africa Against WHO Recommendation. *Res. Rep. Trop. Med.* **2020**, *11*, 61–72. [CrossRef]
13. Santos-Pinto, C.D.B.; Miranda, E.S.; Osorio-de-Castro, C.G.S. O "Kit-Covid" e o Programa Farmácia Popular Do Brasil. *Cad. Saude Publica* **2021**, *37*, e00348020. [CrossRef]
14. Ferreira Caceres, M.M.; Sosa, J.P.; Lawrence, J.A.; Sestacovschi, C.; Tidd-Johnson, A.; Rasool, M.H.U.; Gadamidi, V.K.; Ozair, S.; Pandav, K.; Cuevas-Lou, C.; et al. The Impact of Misinformation on the COVID-19 Pandemic. *AIMS Public Health* **2022**, *9*, 262–277. [CrossRef]
15. Nippes, R.P.; Macruz, P.D.; da Silva, G.N.; Neves Olsen Scaliante, M.H. A Critical Review on Environmental Presence of Pharmaceutical Drugs Tested for the COVID-19 Treatment. *Process Saf. Environ. Prot.* **2021**, *152*, 568–582. [CrossRef]
16. Bartels, I.; Jaeger, M.; Schmidt, T.C. Determination of Anti-SARS-CoV-2 Virustatic Pharmaceuticals in the Aquatic Environment Using High-Performance Liquid Chromatography High-Resolution Mass Spectrometry. *Anal. Bioanal. Chem.* **2023**, *415*, 5365–5377. [CrossRef]
17. Omorogie, M.O.; Babalola, J.O.; Ismaeel, M.O.; McGettrick, J.D.; Watson, T.M.; Dawson, D.M.; Carta, M.; Kuehnel, M.F. Activated Carbon from Nauclea Diderrichii Agricultural Waste—A Promising Adsorbent for Ibuprofen, Methylene Blue and CO_2. *Adv. Powder Technol.* **2021**, *32*, 866–874. [CrossRef]
18. Kumar, M.; Mazumder, P.; Mohapatra, S.; Kumar Thakur, A.; Dhangar, K.; Taki, K.; Mukherjee, S.; Kumar Patel, A.; Bhattacharya, P.; Mohapatra, P.; et al. A Chronicle of SARS-CoV-2: Seasonality, Environmental Fate, Transport, Inactivation, and Antiviral Drug Resistance. *J. Hazard. Mater.* **2021**, *405*, 124043. [CrossRef]
19. Morales-Paredes, C.A.; Rodríguez-Díaz, J.M.; Boluda-Botella, N. Pharmaceutical Compounds Used in the COVID-19 Pandemic: A Review of Their Presence in Water and Treatment Techniques for Their Elimination. *Sci. Total Environ.* **2022**, *814*, 152691. [CrossRef]
20. Kuroda, K.; Li, C.; Dhangar, K.; Kumar, M. Predicted Occurrence, Ecotoxicological Risk and Environmentally Acquired Resistance of Antiviral Drugs Associated with COVID-19 in Environmental Waters. *Sci. Total Environ.* **2021**, *776*, 145740. [CrossRef]

21. Xu, X.; Zhu, R.; Zhang, Y.; Bartelt-Hunt, S.L.; Zou, H.; Chen, C. COVID-19 Related Antiviral Drugs Are Less Adsorbable on Sediment under Alkaline and High Cation Conditions. *Sci. Total Environ.* **2023**, *883*, 163736. [CrossRef]
22. Zhang, J.; Zhan, S.; Zhong, L.-B.; Wang, X.; Qiu, Z.; Zheng, Y.-M. Adsorption of Typical Natural Organic Matter on Microplastics in Aqueous Solution: Kinetics, Isotherm, Influence Factors and Mechanism. *J. Hazard. Mater.* **2023**, *443*, 130130. [CrossRef]
23. Singh, R.; Samuel, M.S.; Ravikumar, M.; Ethiraj, S.; Kirankumar, V.S.; Kumar, M.; Arulvel, R.; Suresh, S. Processing of Carbon-Based Nanomaterials for the Removal of Pollutants from Water/Wastewater Application. *Water* **2023**, *15*, 3003. [CrossRef]
24. Januário, E.F.D.; Fachina, Y.J.; Wernke, G.; Demiti, G.M.M.; Beltran, L.B.; Bergamasco, R.; Vieira, A.M.S. Application of Activated Carbon Functionalized with Graphene Oxide for Efficient Removal of COVID-19 Treatment-Related Pharmaceuticals from Water. *Chemosphere* **2022**, *289*, 133213. [CrossRef]
25. Gonçalves, J.O.; de Farias, B.S.; Rios, E.C.; Ribeiro, A.C.; Acosta, K.d.R.; Gomes, C.P.W.; Cadaval Junior, T.R. Sustainable Removal of Chloroquine from Aqueous Solutions Using Microwave-Activated Cassava Biochar Derived from Agricultural Waste. *Sustainability* **2024**, *16*, 9854. [CrossRef]
26. Vidovix, T.B.; Januário, E.F.D.; Bergamasco, R.; Vieira, A.M.S. Evaluation of Agro-Industrial Residue Functionalized with Iron Oxide Magnetic Nanoparticles for Chloroquine Removal from Contaminated Water. *Mater. Lett.* **2022**, *326*, 132915. [CrossRef]
27. Lindroos, M.; Hörnström, D.; Larsson, G.; Gustavsson, M.; van Maris, A.J.A. Continuous Removal of the Model Pharmaceutical Chloroquine from Water Using Melanin-Covered *Escherichia coli* in a Membrane Bioreactor. *J. Hazard. Mater.* **2019**, *365*, 74–80. [CrossRef]
28. Li, N.; Huo, L.; Shen, W.; Qiang, C.; Wu, M.; Sun, G.; Li, Q.; Shi, M.; Ma, J. Porous Organic Polymers for Superefficient Removal of Pollutants from Water: Design, Synthesis and Adsorption Performance. *J. Clean. Prod.* **2023**, *396*, 136558. [CrossRef]
29. Wang, J.-C.; Guo, J.-T.; Gou, R.-T.; Wang, M.-L.; Wang, Y.-M. Crown Ether-Based Porous Organic Polymers for the Removal of Environmental Pollutants in Water. *J. Incl. Phenom. Macrocycl. Chem.* **2024**, *104*, 1–6. [CrossRef]
30. Yu, T.; Al-Dhabi, N.A.; Xing, W.; Zhu, Y.; Wang, S.; Jiang, K.; Tang, W. Highly Efficient Antibiotic Decontamination and Biotoxicity Elimination with Activity-Stability Considerations via Encapsulated Catalyst Induced Peroxymonosulfate Activation. *J. Environ. Manag.* **2025**, *396*, 128078. [CrossRef]
31. Mary Ealias, A.; Meda, G.; Tanzil, K. Recent Progress in Sustainable Treatment Technologies for the Removal of Emerging Contaminants from Wastewater: A Review on Occurrence, Global Status and Impact on Biota. *Rev. Environ. Contam. Toxicol.* **2024**, *262*, 16. [CrossRef]
32. Kali, A.; Amar, A.; Loulidi, I.; Hadey, C.; Jabri, M.; Alrashdi, A.A.; Lgaz, H.; Sadoq, M.; El-kordy, A.; Boukhlifi, F. Efficient Adsorption Removal of an Anionic Azo Dye by Lignocellulosic Waste Material and Sludge Recycling into Combustible Briquettes. *Colloids Interfaces* **2022**, *6*, 22. [CrossRef]
33. Duarte, M.; Nascimento, G.; Santos, M.; Silva, T.; Campos, N.; Santos, J.; Barbosa, C. Adsorption of Phenol on Adsorbents Produced from Coconut Tree Waste: Kinetic and Equilibrium Studies. *Environ. Eng. Manag. J. (EEMJ)* **2019**, *18*, 693–705. [CrossRef]
34. Demoliner, F.; de Britto Policarpi, P.; Vasconcelos, L.F.L.; Vitali, L.; Micke, G.A.; Block, J.M. Sapucaia Nut (Lecythis Pisonis Cambess) and Its by-Products: A Promising and Underutilized Source of Bioactive Compounds. Part II: Phenolic Compounds Profile. *Food Res. Int.* **2018**, *112*, 434–442. [CrossRef]
35. Silva, A.D.; Oliveira, I.D.N.; Dias, V.L.N.; Mouchrek Filho, V.E.; Carvalho, N.C.C.; Pinheiro, É.M. Anatomical Study and Determination of Active Compounds of the Leaves of Sapucaia (Licythis Pisones). *Rev. Hig. Aliment.* **2011**, *25*, 42–44.
36. Oliveira, J.P.C.; Ferreira, É.L.F.; Chaves, M.H.; Militão, G.C.G.; Júnior, G.M.V.; Costa, A.d.M.; Pessoa, C.d.Ó.; de Moraes, M.O.; Costa-Lotufo, L.V. Chemical Constituents of Lecythis Pisonis and Cytotoxic Activity. *Rev. Bras. Farmacogn.* **2012**, *22*, 1140–1144. [CrossRef]
37. Teixeira, G.L.; Ávila, S.; Hornung, P.S.; Barbi, R.C.T.; Ribani, R.H. Sapucaia Nut (Lecythis Pisonis Cambess.) Flour as a New Industrial Ingredient: Physicochemical, Thermal, and Functional Properties. *Food Res. Int.* **2018**, *109*, 572–582. [CrossRef]
38. Demoliner, F.; de Carvalho, L.T.; de Liz, G.R.; Prudêncio, E.S.; Ramos, J.C.; Bascuñan, V.L.A.F.; Vitali, L.; Block, J.M. Improving the Nutritional and Phytochemical Compounds of a Plant-Based Milk of Sapucaia Nut Cake Using Block Freeze Concentration. *Int. J. Food Sci. Technol.* **2020**, *55*, 3031–3042. [CrossRef]
39. Januário, E.F.D.; Vidovix, T.B.; Bissaro, C.A.; Defendi, R.O.; Jorge, L.M.d.M.; Bergamasco, R.; Vieira, A.M.S. Evaluation of the Black Soybean Hulls Agro-Industrial Waste for Chloroquine Removal from Aqueous Medium and Treatment of Multi-Components. *J. Dispers. Sci. Technol.* **2024**, *45*, 880–890. [CrossRef]
40. Mosoarca, G.; Popa, S.; Vancea, C.; Dan, M.; Boran, S. Removal of Methylene Blue from Aqueous Solutions Using a New Natural Lignocellulosic Adsorbent—Raspberry (Rubus Idaeus) Leaves Powder. *Polymers* **2022**, *14*, 1966. [CrossRef]
41. Newcombe, G.; Hayes, R.; Drikas, M. Granular Activated Carbon: Importance of Surface Properties in the Adsorption of Naturally Occurring Organics. *Colloids Surf. A Physicochem. Eng. Asp.* **1993**, *78*, 65–71. [CrossRef]
42. Li, M.; Tian, X.; Jin, R.; Li, D. Preparation and Characterization of Nanocomposite Films Containing Starch and Cellulose Nanofibers. *Ind. Crops Prod.* **2018**, *123*, 654–660. [CrossRef]

43. Melo, S.d.S.; Diniz, J.E.d.M.; Guimarães, J.H.; Costa, J.d.S.; Brasil, D.d.S.B.; de Morais, S.S.d.S.; Brito, D.C.; Carvalho, J.C.T.; dos Santos, C.B.R.; da Silva, D.L. Production and Characterization of Absorbent Heat from the Bark of Residual Brazil Nut Bark (*Bertholletia excelsa* L.). *Chem. Cent. J.* **2015**, *9*, 36. [CrossRef]
44. Rahmatpour, A.; Soleimani, P.; Mirkani, A. Eco-Friendly Poly(Vinyl Alcohol)/Partially Hydrolyzed Polyacrylamide/Graphene Oxide Semi-IPN Nanocomposite Hydrogel as a Reusable and Efficient Adsorbent of Cationic Dye Methylene Blue from Water. *React. Funct. Polym.* **2022**, *175*, 105290. [CrossRef]
45. Soleimani, S.; Heydari, A.; Fattahi, M.; Motamedisade, A. Calcium Alginate Hydrogels Reinforced with Cellulose Nanocrystals for Methylene Blue Adsorption: Synthesis, Characterization, and Modelling. *Ind. Crops Prod.* **2023**, *192*, 115999. [CrossRef]
46. Zhu, J.; Wang, H.; Guo, F.; Salmén, L.; Yu, Y. Cell Wall Polymer Distribution in Bamboo Visualized with in Situ Imaging FTIR. *Carbohydr. Polym.* **2021**, *274*, 118653. [CrossRef]
47. Cortat, L.O.; Zanini, N.C.; Barbosa, R.F.S.; de Souza, A.G.; Rosa, D.S.; Mulinari, D.R. A Sustainable Perspective for Macadamia Nutshell Residues Revalorization by Green Composites Development. *J. Polym. Environ.* **2021**, *29*, 3210–3226. [CrossRef]
48. Hiew, B.Y.Z.; Lee, L.Y.; Lee, X.J.; Thangalazhy-Gopakumar, S.; Gan, S. Utilisation of Environmentally Friendly Okara-Based Biosorbent for Cadmium(II) Removal. *Environ. Sci. Pollut. Res.* **2021**, *28*, 40608–40622. [CrossRef]
49. Vaghetti, J.C.P.; Lima, E.C.; Royer, B.; da Cunha, B.M.; Cardoso, N.F.; Brasil, J.L.; Dias, S.L.P. Pecan Nutshell as Biosorbent to Remove Cu(II), Mn(II) and Pb(II) from Aqueous Solutions. *J. Hazard. Mater.* **2009**, *162*, 270–280. [CrossRef]
50. Zhou, C.; Qi, S.; Zhu, P.; Zhao, Y.; Xu, Y.; Dong, X.; Wang, D. The Methylene Infrared Vibration and Dielectric Behavior Monitored by Amide Group Arrangement for Long Chain Polyamides. *Polymer* **2020**, *190*, 122231. [CrossRef]
51. Bansal, R.C.; Goyal, M. *Activated Carbon Adsorption*; CRC Press: Boca Raton, FL, USA, 2005; ISBN 9781420028812.
52. Usman, M.A.; Momohjimoh, I.; Usman, A.O. Characterization of Groundnut Shell Powder as a Potential Reinforcement for Biocomposites. *Polym. Renew. Resour.* **2021**, *12*, 77–91. [CrossRef]
53. Fellak, S.; Rafik, M.; Haidara, H.; Boukir, A.; Lhassani, A. Study of Natural Degradation Effect on Lignocellulose Fibers of Archaeological Cedar Wood: Monitoring by Fourier Transform Infrared (FTIR) Spectroscopy. *MATEC Web Conf.* **2022**, *360*, 00006. [CrossRef]
54. Usman, M.O.; Aturagaba, G.; Ntale, M.; Nyakairu, G.W. A Review of Adsorption Techniques for Removal of Phosphates from Wastewater. *Water Sci. Technol.* **2022**, *86*, 3113–3132. [CrossRef]
55. Islam, M.A.; Chowdhury, M.A.; Mozumder, M.S.I.; Uddin, M.T. Langmuir Adsorption Kinetics in Liquid Media: Interface Reaction Model. *ACS Omega* **2021**, *6*, 14481–14492. [CrossRef]
56. Ho, Y.S.; McKay, G. A Comparison of Chemisorption Kinetic Models Applied to Pollutant Removal on Various Sorbents. *Process Saf. Environ. Prot.* **1998**, *76*, 332–340. [CrossRef]
57. Ferreira, I.A.; Wernke, G.; Diório, A.; Bergamasco, R.; Vieira, M. Sunflower Seed Husks as a Cost-Effective Adsorbent for Chloroquine Removal from Water. *Rev. Bras. Ciênc. Ambient.* **2024**, *59*, e1907. [CrossRef]
58. Santos, R.K.S.; Nascimento, B.F.; de Araújo, C.M.B.; Cavalcanti, J.V.F.L.; Bruckmann, F.S.; Rhoden, C.R.B.; Dotto, G.L.; Oliveira, M.L.S.; Silva, L.F.O.; Motta Sobrinho, M.A. Removal of Chloroquine from the Aqueous Solution by Adsorption onto Açaí-Based Biochars: Kinetics, Thermodynamics, and Phytotoxicity. *J. Mol. Liq.* **2023**, *383*, 122162. [CrossRef]
59. Sun, H.; He, J.; Liu, Y.; Ji, X.; Wang, G.; Yang, X.; Zhang, Y. Removal Performance and Mechanism of Emerging Pollutant Chloroquine Phosphate from Water by Iron and Magnesium Co-Modified Rape Straw Biochar. *Molecules* **2023**, *28*, 3290. [CrossRef]
60. Weber, W.J.; Morris, J.C. Advances in Water Pollution Research: Removal of Biologically Resistant Pollutant from Wastewater by Adsorption. In *Proceedings of the 1st International Conference on Water Pollution Symposium*; Pergamon Press: London, UK, 1962.
61. de Souza, R.M.; Magalhães-Ghiotto, G.A.V.; Bergamasco, R. Enhanced Chloroquine Adsorption Using Cobalt-Modified Mesoporous Silicas for Water Treatment. *Chem. Eng. Process.-Process Intensif.* **2025**, *210*, 110224. [CrossRef]
62. Lima, É.C.; Adebayo, M.A.; Machado, F.M. *Kinetic and Equilibrium Models of Adsorption*; Springer International Publishing: Cham, Switzerland, 2015; pp. 33–69.
63. Tanase, C.; Coșarcă, S.; Muntean, D.-L. A Critical Review of Phenolic Compounds Extracted from the Bark of Woody Vascular Plants and Their Potential Biological Activity. *Molecules* **2019**, *24*, 1182. [CrossRef]
64. Das, A.K.; Islam, M.N.; Faruk, M.O.; Ashaduzzaman, M.; Dungani, R. Review on Tannins: Extraction Processes, Applications and Possibilities. *S. Afr. J. Bot.* **2020**, *135*, 58–70. [CrossRef]
65. Antony, A.; Farid, M. Effect of Temperatures on Polyphenols During Extraction. *Appl. Sci.* **2022**, *12*, 2107. [CrossRef]
66. Akpa, O.M.; Unuabonah, E.I. Small-Sample Corrected Akaike Information Criterion: An Appropriate Statistical Tool for Ranking of Adsorption Isotherm Models. *Desalination* **2011**, *272*, 20–26. [CrossRef]
67. Oreofe, T.A.; Inyinbor, A.A.; Bello, O.S.; Ogunleye, O.O. Adsorption Isotherm, Kinetics and Thermodynamics Studies on Chloroquine Sequestration Using Coconut Shell Activated Carbon. In Proceedings of the 2024 International Conference on Science, Engineering and Business for Driving Sustainable Development Goals (SEB4SDG), Omu-Aran, Nigeria, 2–4 April 2024; pp. 1–6. [CrossRef]

68. Bankole, D.T.; Oluyori, A.P.; Inyinbor, A.A. Acid-Activated Hibiscus Sabdariffa Seed Pods Biochar for the Adsorption of Chloroquine Phosphate: Prediction of Adsorption Efficiency via Machine Learning Approach. *S. Afr. J. Chem. Eng.* **2022**, *42*, 162–175. [CrossRef]
69. Tran, H.N.; You, S.-J.; Chao, H.-P. Thermodynamic Parameters of Cadmium Adsorption onto Orange Peel Calculated from Various Methods: A Comparison Study. *J. Environ. Chem. Eng.* **2016**, *4*, 2671–2682. [CrossRef]
70. Elliott, J.R.; Lira, C.T. *Introductory Chemical Engineering Thermodynamics*; Prentice Hall: Hoboken, NJ, USA, 2012.
71. Liu, Y. Is the Free Energy Change of Adsorption Correctly Calculated? *J. Chem. Eng. Data* **2009**, *54*, 1981–1985. [CrossRef]
72. Zhang, Y.; Zhu, C.; Liu, F.; Yuan, Y.; Wu, H.; Li, A. Effects of Ionic Strength on Removal of Toxic Pollutants from Aqueous Media with Multifarious Adsorbents: A Review. *Sci. Total Environ.* **2019**, *646*, 265–279. [CrossRef]
73. Karić, N.; Maia, A.S.; Teodorović, A.; Atanasova, N.; Langergraber, G.; Crini, G.; Ribeiro, A.R.L.; Đolić, M. Bio-Waste Valorisation: Agricultural Wastes as Biosorbents for Removal of (in)Organic Pollutants in Wastewater Treatment. *Chem. Eng. J. Adv.* **2022**, *9*, 100239. [CrossRef]
74. Baskar, A.V.; Bolan, N.; Hoang, S.A.; Sooriyakumar, P.; Kumar, M.; Singh, L.; Jasemizad, T.; Padhye, L.P.; Singh, G.; Vinu, A.; et al. Recovery, Regeneration and Sustainable Management of Spent Adsorbents from Wastewater Treatment Streams: A Review. *Sci. Total Environ.* **2022**, *822*, 153555. [CrossRef]
75. Kong, X.; Li, Y.; Liu, X. A Review of Thermosensitive Antinutritional Factors in Plant-Based Foods. *J. Food Biochem.* **2022**, *46*, e14199. [CrossRef]
76. Hashem, A.; Aniagor, C.O.; Morsy, O.M.; Abou-Okeil, A.; Aly, A.A. Apricot Seed Shell: An Agro-Waste Biosorbent for Acid Blue193 Dye Adsorption. *Biomass Convers. Biorefin.* **2024**, *14*, 12283–12296. [CrossRef]
77. Saadi, A.S.; Slimane Ben Ali, D.; Bousba, S. Utilization of a Biosorbent Derived from Plant Residues for the Treatment of Water Contaminated with Rhodamine B: Preparation and Characterization. *RSC Adv.* **2025**, *15*, 43038–43052. [CrossRef]
78. Azizian, S. Kinetic Models of Sorption: A Theoretical Analysis. *J. Colloid Interface Sci.* **2004**, *276*, 47–52. [CrossRef]
79. Simonin, J.-P. On the Comparison of Pseudo-First Order and Pseudo-Second Order Rate Laws in the Modeling of Adsorption Kinetics. *Chem. Eng. J.* **2016**, *300*, 254–263. [CrossRef]

Disclaimer/Publisher's Note: The statements, opinions and data contained in all publications are solely those of the individual author(s) and contributor(s) and not of MDPI and/or the editor(s). MDPI and/or the editor(s) disclaim responsibility for any injury to people or property resulting from any ideas, methods, instructions or products referred to in the content.